Journal of Constructional Steel Research 224 (2025) 109069

Contents lists available at ScienceDirect

Journal of Constructional Steel Research

journal homepage: www.elsevier.com/locate/jcsr

Testing and design of wire and arc additively manufactured steel double-shear bolted connections with thick plates

Yunyi Liu [a], Jun Ye [b,*], Jiangfei He [c], Hongjia Lu [a], Guan Quan [a,*], Zhen Wang [d], Yang Zhao [e]

[a] College of Civil Engineering and Architecture, Zhejiang University, Hangzhou 310058, China
[b] School of Civil Engineering, University of Leeds, Leeds LS2 9JT, UK
[c] China Energy Engineering Group, Zhejiang Electric Power Design Institute Co. Ltd, Hangzhou 310012, China
[d] Department of Civil Engineering, Hangzhou City University, Hangzhou 310015, China
[e] School of Civil Engineering, Shaoxing University, Shaoxing, China

ARTICLE INFO

Keywords:
Metal 3D printing
Wire arc additive manufacturing
Double-shear bolt connections
Failure modes
Design approaches

ABSTRACT

The integration of additive manufacturing technology into the construction sector has attracted considerable interest in recent years. However, despite the increasing demand for large-scale constructions subjected to large forces, the research on the structural behaviour of thick plates fabricated via Wire and Arc Additive Manufacturing (WAAM) technology has been limited. This paper investigated the structural behaviour and design of WAAM carbon steel double-shear bolted connections with thick plates. The experiment examined 30 bolted connections with varying geometric dimensions and print layer orientations, discovering failure modes including net section tension, shear-out, end-splitting, and bearing failure. The research revealed anisotropic behaviours in WAAM steel bolted connections, with different print layer orientations affecting their failure modes and ultimate capacities. It is consistent with the inherent anisotropy observed in WAAM steel materials. Furthermore, the experimental results were analysed and compared with predictions made by existing design approaches for conventional steel bolted connections. While the existing guidelines were found to be applicable to WAAM steel bolted connections, certain limitations were identified.

1. Introduction

In recent years, additive manufacturing has gained prominence within the manufacturing industry, providing new possibilities that complement traditional manufacturing processes. This cutting-edge technology, commonly known as 3D printing, enables the production of intricate geometries that traditional methods find challenging or unfeasible. Among various additive manufacturing techniques, Wire Arc Additive Manufacturing (WAAM) stands out for its efficiency, cost-effectiveness, and sustainability in fabricating large-scale and complex steel structures [1–8]. This has gained significant interest, particularly in the field of Civil Engineering. WAAM employs an electric arc to melt the wire feedstock, which is then deposited layer by layer to create the desired structure on the substrate plate, as depicted in Fig. 1. Early notable applications of WAAM technology, illustrated in Fig. 2, include the construction of topology-optimized cantilever trusses, hooks, bolted connections, and WAAM steel footbridges, highlighting its potential as a transformative manufacturing process.

As the application of WAAM technology in construction continues to gain traction, acquiring a comprehensive understanding of the material properties of plates produced via WAAM has become increasingly important. Extensive studies have been conducted on the material properties of WAAM steel across various types, including stainless steels and carbon steels [12–25]. Based on these experiments, the research has also emerged on establishing the constitutive models for WAAM steels [26]. Not only limited to the material properties, the structural behaviours of WAAM structures among beams, columns, connections, and other structural elements [10,27–35] have also been studied. Particularly, the structural behaviours of bolted connections in WAAM steel structures have warranted an in-depth investigation, especially concerning the limitations inherent to the WAAM process.

Due to manufacturing limitations and dimensional constraints, large-scale metallic structures produced via WAAM technology need to be printed in parts and assembled using bolted connections. Extensive research has investigated the structural behaviours of bolted connections in conventionally produced steels [36–40], revealing that

* Corresponding authors.
E-mail addresses: J.Ye2@leeds.ac.uk (J. Ye), guan.quan@zju.edu.cn (G. Quan).

https://doi.org/10.1016/j.jcsr.2024.109069
Received 10 July 2024; Received in revised form 5 September 2024; Accepted 28 September 2024
Available online 23 October 2024

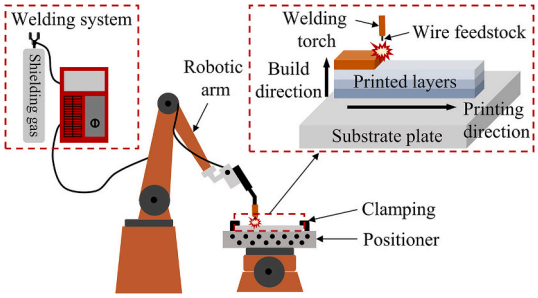

Fig. 1. Manufacturing equipment and the printed structure of WAAM process.

geometric features such as plate width, end distance, and plate thickness significantly affect their ultimate capacities and failure modes. Design provisions have been established for bolted connections in conventional steel with various failure modes [41–47]. However, studies on WAAM steel bolted connections remain limited. The structural behaviours of WAAM carbon steel bolted connections [18,19,48,49] and stainless steel bolted connections [50,51] were investigated. The design guidelines of conventionally manufactured steel bolted connections [52–56] were utilized to evaluate the ultimate capacities of WAAM steel bolted connections, despite of the inherent differences in material properties. The increasing demand for thicker steel plates in structures, such as buildings and bridges, has contributed to highly attention on connections between these plates. For thick plates produced via WAAM, different printing strategies and parameters have been employed, potentially leading to varied responses and adaptation challenges to existing design provisions compared to thin plates. To further promote the development of design guidelines for WAAM steel bolted connections with thick plates, more tests and analyses are needed.

This study conducted an experimental investigation to examine the mechanical properties and structural behaviours of WAAM carbon steel plates and double-shear WAAM steel bolted connections under monotonic loading. Thirty double-shear bolted connection specimens, consisting of thick plates with a nominal thickness of 8 mm and varying print layer orientations and geometric dimensions, were tested. The geometric dimensions of these specimens were obtained using a 3D laser scanner, while Digital Image Correlation (DIC) was employed to monitor the displacements during testing. The study analysed the effects of print layer orientations on the ultimate capacities and failure modes of bolted connections. Test results were compared with predictions based on existing design provisions for conventional steel structures to assess their applicability to WAAM steel. This research enhances understanding of the material properties and structural behaviours of WAAM steel bolted connections, thereby advancing the integration of 3D printing technology in construction.

2. Existing design equations for bolted connections

While design provisions for 3D-printed bolted connections have yet to be established, existing provisions for conventionally manufactured steel can be adapted to accommodate the unique material properties of WAAM steel. In particular, for connections with a nominal plate thickness exceeding 8 mm, the relevant design provisions are reviewed and assessed for applicability.

2.1. AS 4100 [52]

The AS 4100 [52] standard, developed by Standards Australia Committee for steel structures, provides guidelines for calculating the ultimate capacities of bolted connections. For specimens with varying geometric features shown in Fig. 3, the ultimate capacities of net section tension failure mode can be calculated using Eq. (1a). Whilst for shear-out failure and bearing failure, the ultimate capacities are calculated using Eqs. (1b) and (1c), respectively. The final capacity for a specific connection is taken as the lowest value among these calculated

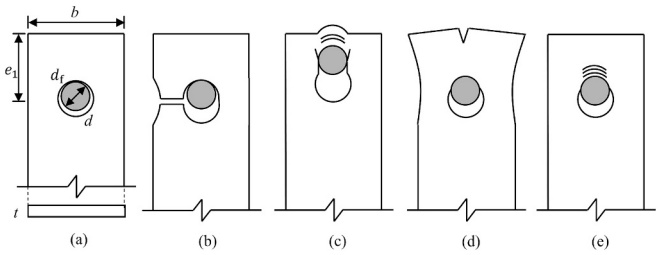

Fig. 3. A bolted connection specimen and corresponding failure modes: (a) the geometric features, (b) net section tension, (c) shear-out, (d) end-splitting, and (e) bearing failure.

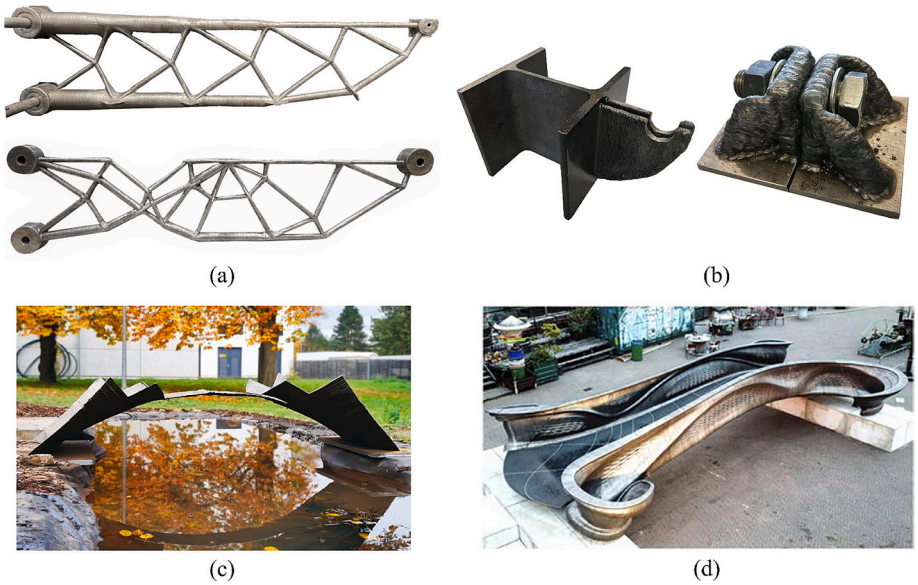

Fig. 2. WAAM steel structures: (a) the topology-optimized cantilever trusses [2,9], (b) the topology-optimized hook and bolted connection [10], (c) a WAAM footbridge in shell form [11], and (d) a MX3D WAAM footbridge [6].

Table 1
Printing and environmental parameters of specimens with a nominal thickness of 8 mm.

Travel speed (m/min)	Wire feed rate (m/min)	Wire diameter (mm)	Welding voltage (V)	Layer thickness (mm)	Bead width (mm)	Temperature (°C)	Humidity (% RH)	Shielding gas
0.55–0.6	6.5	1.2	23	2.7	7.5	12–21	35–55	97 %Ar + 3 % CO_2

capacities.

$$F_{ns,AS} = 0.85A_n f_u \tag{1a}$$

$$F_{so,AS} = \left(e_1 - \frac{d}{2}\right) t f_u \tag{1b}$$

$$F_{b,AS} = 3.2 d_f t f_u \tag{1c}$$

where A_n is the net sectional area of the connection plate; f_u denotes the tensile strength of the connection plate; e_1 is the distance between the centre of a standard bolt hole to the end of the connection plate; t is the thickness of the connection plates; d is the nominal bolt hole diameter; and d_f is the nominal bolt diameter.

2.2. AISC 360 [55]

The AISC 360:2020 [55], developed by the American National Standards Institute for structural steel buildings, provides a similar approach to the AS 4100 code [52] for determining the nominal capacities of a connection. The nominal capacity is determined as the lowest value for the net section tension, shear-out, and bearing failure modes, which are shown in Eqs. (2a), (2b) and (2c), respectively.

$$F_{ns,AISC} = A_n f_u \tag{2a}$$

$$F_{so,AISC} = 1.5\left(e_1 - \frac{d}{2}\right) t f_u \tag{2b}$$

$$F_{b,AISC} = 3 d_f t f_u \tag{2c}$$

2.3. Eurocode 3 [53,54]

Eurocode 3 [53,54] is developed by the British Standards Institution for steel structures. The ultimate capacity of net section tension failure mode can be calculated using Eq. (3a) proposed by EN 1993-1-1:2020 [53]. For bearing failure, the ultimate capacity is calculated using Eq. (3b) proposed by EN 1993-1-8:2021 [54]. The final capacity for a specific connection is the lowest value among the two capacities.

$$F_{ns,EN1} = k A_n f_u \tag{3a}$$

$$F_{EN8} = \alpha_b k_m d_f t f_u \tag{3b}$$

where $k = 1$, for plates with smooth holes fabricated by drilling or water jet cutting; or $k = 0.9$, for plates with rough holes fabricated by punching or flame cutting; α_b is the minimum of e_1/d, $3f_{ub}/f_u$, and 3; for steel grades equal to or higher than S460, $k_m = 0.9$; otherwise, $k_m = 1$.

2.4. Design equations proposed in the literature

For shear-out failure mode, different design codes employ various shear failure planes. The AS/NZS 4600 [56] standard adopts the gross shear length ($L_{gv} = e_1$), whereas AS 4100 [52] uses the net shear length ($L_{nv} = e_1$-$d/2$). Teh and Uz [44] proposed Eq. (4), defining an active shear length ($L_{av} = e_1$-$d/4$) based on their experimental and numerical analyses. Based on the proposed active shear length, Eq. (5) was proposed by Xing et al. [45], considering the catenary action which has a significant effect on the shear-out capacity.

$$F_{so} = 1.2\left(e_1 - \frac{d}{4}\right) t f_u \tag{4}$$

$$F_{so} = 1.2\left(\frac{3d_f}{e_1}\right)^p \left(e_1 - \frac{d}{4}\right) t f_u \tag{5}$$

Similar to the shear-out failure mode, the design equations for bearing failure mode in various codes employ different bearing coefficients. AS 4100 [52] adopts a coefficient of 3.2, while AISC 360 [55] uses a coefficient of 3. Based on the analysis of experimental data, Teh and Uz [38] proposed a higher bearing coefficient of 3.5, which is incorporated into Eq. (6).

$$F_b = 3.5 d_f t f_u \tag{6}$$

3. Experimental programme

3.1. Materials and specimens

In the experiment, two types of steel plates with a nominal thickness of 8 mm were utilized: WAAM steel plates and high-strength Q690 steel plates. The test WAAM steel plate was manufactured using WAAM technology, following the printing parameters listed in Table 1. The

Table 2
Chemical compositions (% by weight) of ER50–6 low carbon steel feedstock.

Chemical compositions	C	Mn	Si	P	S	Cr	Ni	Cu	Mo	V
ER50–6	0.074	1.47	0.85	0.015	0.01	0.023	0.009	0.1	0.004	0.002

Table 3
Mechanical properties of ER50–6 low carbon steel feedstock.

	Tensile Strength (MPa)	Yield Strength (MPa)	Elongation Rate (%)	Charpy V Impact Test Value at 40 °C (J)
ER50–6	554	445	26	96

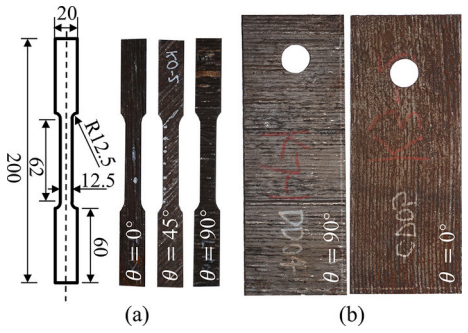

Fig. 4. Examples of (a) tensile coupons and (b) bolted connection specimens with different angles θ to the print layer orientation.

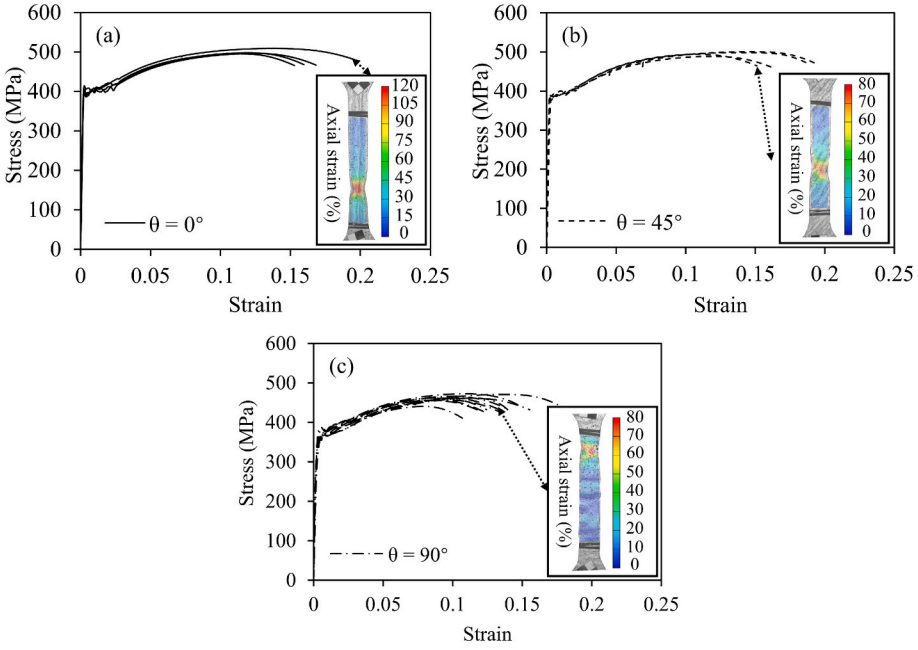

Fig. 5. The stress-strain curves of coupons with θ of (a) 0°, (b) 45°, and (c) 90°.

Table 4
Average material properties for coupons with a nominal thickness of 8 mm.

Nominal thickness (mm)	Actual thickness (mm)	θ (°)	E (GPa)	f_y (MPa)	f_u (MPa)	ε_u	ε_f	$\frac{f_{y,\theta}}{f_{y,\theta=0°}}$	$\frac{f_{u,\theta}}{f_{u,\theta=0°}}$	$\frac{\varepsilon_{u,\theta}}{\varepsilon_{u,\theta=0°}}$	$\frac{\varepsilon_{f,\theta}}{\varepsilon_{f,\theta=0°}}$
8	8.9	0	206	393	500	0.12	0.17	1.00	1.00	1.00	1.00
	8.3	45	196	386	496	0.13	0.17	0.98	0.99	1.03	1.03
	8.6	90	182	364	461	0.10	0.14	0.93	0.92	0.81	0.80

feedstock used was ER50–6 low-carbon steel, whose chemical composition and mechanical properties, as provided by the manufacturer, are listed in Tables 2 and 3, respectively. The test high-strength Q690 steel plates with a measured yield strength $f_{y,HSS}$= 793 MPa and a measured tensile strength $f_{u,HSS}$= 854 MPa were used.

Tensile coupon tests were undertaken to obtain the basic material properties of the WAAM steel bolted connections. A total of 19 as-built coupons were tested, including 4 coupons with a θ of 0°, 4 coupons with a θ of 45°, and 11 coupons with a θ of 90°. These tests were conducted on a 250 kN Instron 8802 testing machine using displacement control mode at a stroke rate of 0.8 mm/min. Tensile coupons with three print layer orientations, as shown in Fig. 4(a), were tested to investigate the influence of print layer orientations on the mechanical properties of WAAM steel.

The stress-strain curves and material properties of tensile coupons are shown in Fig. 5 and Table 4, respectively. It is evident that WAAM steel exhibited a degree of anisotropy, characterized by the gradual disappearance of yielding plateaus in the stress-strain curves with increasing θ, and a general decrease in material properties with higher θ values. The yield and ultimate stress of coupons at 0° and 90° specimens showed differences of 7 % and 8 %, respectively. Moreover, a larger disparity of approximately 20 % was observed between the ultimate tensile strain and fracture strain of the 0° and 90° specimens, indicating significant differences in ductility and fracture performance based on the print layer orientation.

A total of 30 WAAM steel bolted connection specimens with varying geometric dimensions and two different print layer orientations were designed, as shown in Fig. 4(b). For each group of specimens with specific geometric dimensions, two specimens with θ angles of 0° and 90° were manufactured to study potential anisotropy.

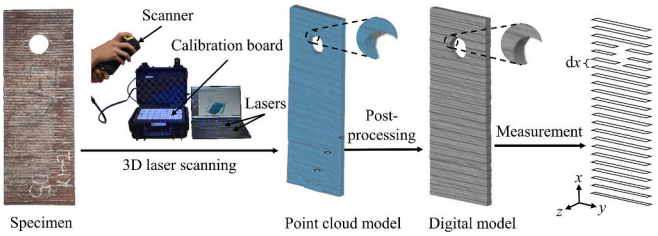

Fig. 6. The process of scanning, post processing, and measurement.

The actual geometric dimensions of WAAM steel bolted connection specimens were measured using a 3D laser scanner, SIMSCAN from SCANTECH, due to the undulating surfaces of the WAAM steel plates. Fig. 6 illustrates the whole process of scanning, post-processing, and measurement. The point cloud model was obtained by scanning the test specimen, which underwent post-processing to eliminate errors and repair imperfections, forming the 3D digital model. Contouring of each digital model was performed at regular intervals (dx = 0.1 mm [18]) along the X-axis to determine the geometric dimensions at each cross-sectional cut and derive the final geometric dimensions of the tested specimen. More detailed measurement process was described by Liu et al. [19].

The measurement results are shown in Table 5. The high-strength steel plates were measured in the same way, and their measurement results are also listed in Table 5. Each steel plate was named using the form of HD8-d-b-e_1, VD8-d-b-e_1, or HSS-d-b-e_1 with nominal dimensions. The letter 'H' or 'V' indicates that the plate was extracted horizontally or vertically relative to the print layer orientation, with θ being 0° or 90°, respectively. The letter 'D' denotes the double-shear connection type,

Table 5
Geometric dimensions of WAAM and high-strength steel connected plates.

Specimens	d_f (mm)	t (mm)	d (mm)	b (mm)	e_1 (mm)	Predictive failure modes*	Matched specimens	t_{HSS} (mm)	d_{HSS} (mm)	b_{HSS} (mm)	$e_{1,HSS}$ (mm)
HD8–26–70-39	24.0	8.4	26.0	69.9	39.0	SO	HSS8–26–70-39	8.0	26.6	70.8	39.7
VD8–26–70-39	24.0	8.2	25.8	69.7	38.7	SO		7.9	25.9	70.5	38.2
HD8–26–90-39	24.0	8.1	26.0	90.3	39.2	SO	HSS26–90-39	7.9	26.6	90.2	39.2
VD8–26–90-39	24.0	8.5	26.2	89.8	38.5	SO		8.0	26.6	90.2	38.6
HD8–26–100-52	24.0	8.8	26.2	100.0	51.5	SO	HSS8–26–100-52	7.9	26.5	100.5	48.1
VD8–26–100-52	24.0	8.0	26.2	100.4	51.5	SO		8.0	26.0	100.4	52.1
HD8–26–100-58	24.0	8.5	26.0	99.6	56.8	SO	HSS8–26–100-58	8.0	26.3	100.9	57.0
VD8–26–100-58	24.0	8.2	25.8	100.2	57.1	SO		8.0	25.8	100.8	58.0
HD8–26–100-73	24.0	8.4	26.0	100.4	72.4	B	HSS8–26–100-73	7.9	26.4	100.6	73.8
VD8–26–100-73	24.0	8.4	25.8	100.1	72.7	B		7.9	26.0	100.6	72.7
HD8–26–110-78	24.0	8.5	26.0	110.7	77.0	B	HSS8–26–110-78	8.0	26.5	111.0	77.7
VD8–26–110-78	24.0	8.2	26.0	110.1	77.7	B		8.3	26.3	110.2	78.4
HD8–26–110-84	24.0	8.6	26.2	110.2	82.5	B	HSS8–26–110-84	8.0	26.6	110.4	83.5
VD8–26–110-84	24.0	8.9	25.8	110.0	83.3	B		7.9	26.4	110.6	83.7
HD8–32–70-48	30.0	8.7	32.8	70.3	47.4	NS	HSS8–32–70-48	7.9	32.3	70.2	48.9
VD8–32–70-48	30.0	8.8	32.8	70.2	47.6	NS		7.9	31.9	70.7	47.6
HD8–32–90-48	30.0	8.4	32.2	90.0	47.7	NS	HSS8–32–90-48	8.0	32.2	90.7	48.5
VD8–32–90-48	30.0	8.1	32.0	89.5	48.6	NS		8.0	32.0	90.6	48.0
HD8–32–120-90	30.0	8.4	32.4	120.9	89.0	SO	HSS8–32–120-90	8.0	32.2	120.3	90.6
VD8–32–120-90	30.0	8.7	32.2	12.0	90.9	SO		7.9	32.0	120.1	90.4
HD8–32–130-96	30.0	8.3	32.0	130.3	95.8	NS	HSS8–32–130-96	8.0	32.4	130.8	96.0
VD8–32–130-96	30.0	7.9	31.8	130.5	93.9	NS		8.0	32.1	131.1	95.7
HD8–32–100-80	30.0	8.4	32.2	99.7	77.3	B	HSS8–32–100-80	8.0	32.9	100.4	80.9
VD8–32–100-80	30.0	9.2	32.0	99.2	79.8	B		8.0	31.6	100.4	79.6
HD8–32–110-80	30.0	8.8	32.2	111.3	79.3	NS	HSS8–32–110-80	7.9	31.5	111.3	80.6
VD8–32–110-80	30.0	8.0	32.0	110.0	79.0	NS		7.9	31.7	110.6	80.1
HD8–32–120-77	30.0	8.2	32.0	120.5	76.6	NS	HSS8–32–120-77	7.9	32.4	120.2	77.4
VD8–32–120-77	30.0	9.3	32.4	120.4	76.6	NS		7.9	32.2	120.6	77.1
HD8–32–130-87	30.0	8.7	32.4	131.1	86.4	NS	HSS8–32–130-87	8.0	32.2	130.1	87.0
VD8–32–130-87	30.0	8.7	32.0	130.2	86.0	NS		8.1	32.0	131.2	86.8

Note: NS = net section tension failure; SO = shear-out; ES = end-splitting failure; B = bearing failure.
* Predictive failure modes were predicted by AISC 360 [55] as an example.

followed by the nominal thickness t of 8 mm. "HSS" stands for high-strength steel.

3.2. Test arrangements

The experiments were performed with a 1000 kN Instron 8805 testing machine operating in displacement control mode at a stroke rate of 1.0 mm/min. The test setup is depicted in Fig. 7. The specimens tested were single-bolt double-shear connections, each composed of a WAAM steel plate and a pair of corresponding high-strength steel plates. These components were bolted together in a 2 mm clearance hole using bolts tightened by hand. Bolts of grade 12.9, with nominal diameters of 24 mm and 30 mm, were employed. To ensure the application of concentric loads, auxiliary plates were attached at the clamping end of the specimens.

The displacement of the bolted connection specimen was measured by tracking the displacement of the unfixed plate using a Digital Image Correlation (DIC) system, complemented by an extensometer with a gauge length of 150 mm. This DIC system provided non-contact, full-field measurements at a frequency of 5 Hz. To facilitate displacement tracking, each specimen was painted with an alternating white and black pattern, generating a random speckle design. The displacement fields at different displacements obtained by the DIC system for are displayed in Fig. 8.

4. Double-shear connection tests

4.1. Test result

The detailed test results for all double-shear bolted connection

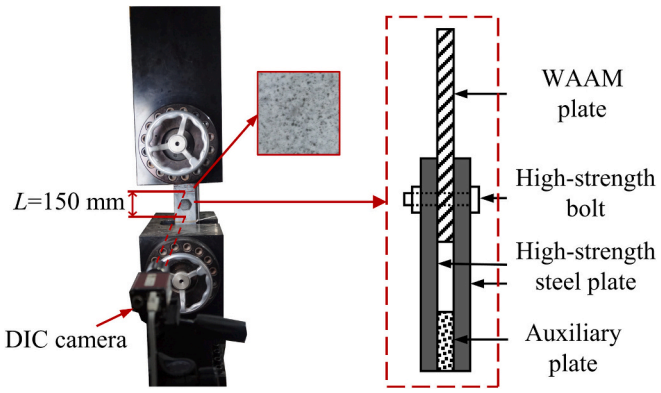

Fig. 7. The test setup.

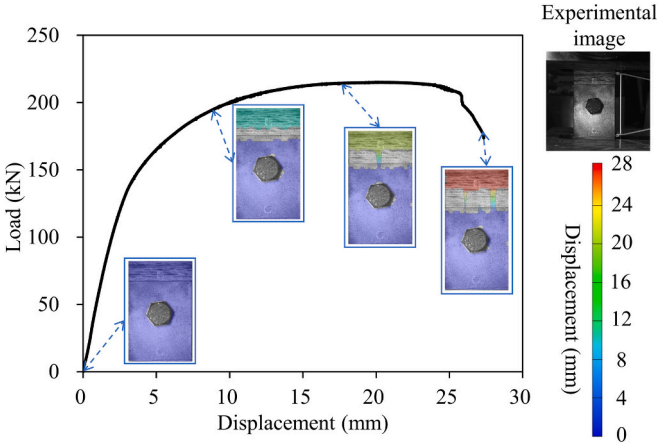

Fig. 8. Displacement fields at different displacements.

specimens are summarized in Table 6. This table systematically arranges each pair of specimens with identical nominal dimensions but different print layer orientations in the same row. The ultimate capacity F_u was taken as the maximum load measured in tests. The F_u values ranged from 152.1 kN to 385.2 kN, leading to different failure modes, including net section tension, shear-out, end-splitting, and bearing failure. Fig. 9 presents the photos of the four failure modes observed in the tests.

Specimens that failed due to net section tension typically exhibited necking across the width and thickness of the plates, as shown in Fig. 9 (a). In contrast, specimens failing due to shear-out showed hole elongation, longitudinal tears (i.e., aligned with the direction force of application), and material accumulation, as depicted in Fig. 9(b). Specimens failing due to end-splitting experienced high transverse stress and showed fractures originating from the plate end, progressively extending towards the bolt hole, as demonstrated in Fig. 9(c). Unlike the thin specimens that displayed bearing failure, the material in front of the bolt hole in the thick plates was difficult to pile up under the compression of the bolt, resulting in material being forced outward and extruded from the plate end, as shown in Fig. 9(d).

The experimental observations revealed that certain HD specimens exhibited a hybrid failure mode of shear-out and end-splitting. This mode was characterized by a tensile fracture at the specimen's tip and a shear fracture along the elongated region, as depicted in Fig. 10. The hybrid failure mode can be attributed to the simultaneous presence of high transverse and axial stresses within the specimens.

Fig. 11 shows the load-displacement curves of test specimens grouped by different failure modes. The load-displacement curves for specimens with varying widths that failed in net section tension indicate that both the ultimate bearing capacity and displacement increase with the width, as shown in Fig. 11(a). However, VD8–32–120-90 and VD8–26–110-84 exhibited anomalous displacement behaviour. The failure patterns of these two specimens suggested that fractures occurred between the print layers, as shown in Fig. 12. These specimens were expected to experience bearing failure, but they underwent premature net section tension failure, resulting in larger displacements compared to the typical net section tension failure. This anomaly could be attributed to the undulating surfaces of WAAM specimens, which caused defects leading to a shift in the failure mode. For the ten specimens that have undergone the hybrid failure of shear-out and end-splitting, ultimate capacities and displacements were generally positively correlated with the end distances, as shown in Fig. 11(b). In contrast, for the ten bearing failure specimens, the ultimate capacities and displacements did not vary significantly with different widths and end distances, as demonstrated in Fig. 11(c).

4.2. Analysis of anisotropy behaviours

For the 15 pairs of specimens with the identical nominal dimensions but different print layer orientations, anisotropic behaviours were observed. The normalized ultimate capacity ratios $F_{u,90°}/tf_{u,90°}$ and $F_{u,0°}/tf_{u,0°}$ of the VD and HD specimens are compared in Fig. 13, categorized by failure modes.

Overall, the normalized ultimate capacity ratios ranged between 1.0 and 1.2, indicating that the ultimate capacities of VD specimens were generally higher than those of HS specimens of the same dimensions, which suggests a clear anisotropic behaviour. This anisotropy was further evidenced by the inconsistency in failure modes between specimen pairs. In the case of specimen pairs No. 1–4, a notable deviation in the general failure modes trends was observed. VD specimens tended to exhibit end-splitting failure, while HD specimens were more likely to

Table 6
Test results for double-shear bolted connection specimens.

No.	Specimen	Failure mode	$F_{u,0°}$ (kN)	Specimen	Failure mode	$F_{u,90°}$ (kN)	$F_{u,90°}/F_{u,0°}$
1	HD8–26–70-39	SO/ES	166.7	VD8–26–70-39	SO	160.9	0.97
2	HD8–26–90-39	SO/ES	152.7	VD8–26–90-39	SO	160.8	1.05
3	HD8–26–100-52	SO/ES	226.5	VD8–26–100-52	SO	215.2	0.95
4	HD8–26–100-58	ES	250.3	VD8–26–100-58	SO	241.4	0.96
5	HD8–26–100-73	B	296.4	VD8–26–100-73	NS	290.4	0.98
6	HD8–26–110-78	B	328.5	VD8–26–110-78	B	321.2	0.98
7	HD8–26–110-84	B	356.6	VD8–26–110-84	NS	374.2	1.05
8	HD8–32–70-48	NS	159.7	VD8–32–70-48	NS	152.1	0.95
9	HD8–32–90-48	SO/ES	202.3	VD8–32–90-48	NS	202.5	1.00
10	HD8–32–100-80	NS	278.9	VD8–32–100-80	NS	318.0	1.14
11	HD8–32–110-80	NS	319.3	VD8–32–110-80	NS	311.3	0.97
12	HD8–32–120-77	B	315.9	VD8–32–120-77	B	385.2	1.22
13	HD8–32–120-90	B	363.2	VD8–32–120-90	NS	372.2	1.02
14	HD8–32–130-87	SO/ES	364.3	VD8–32–130-87	B	361.3	0.99
15	HD8–32–130-96	B	378.7	VD8–32–130-96	B	377.0	1.00

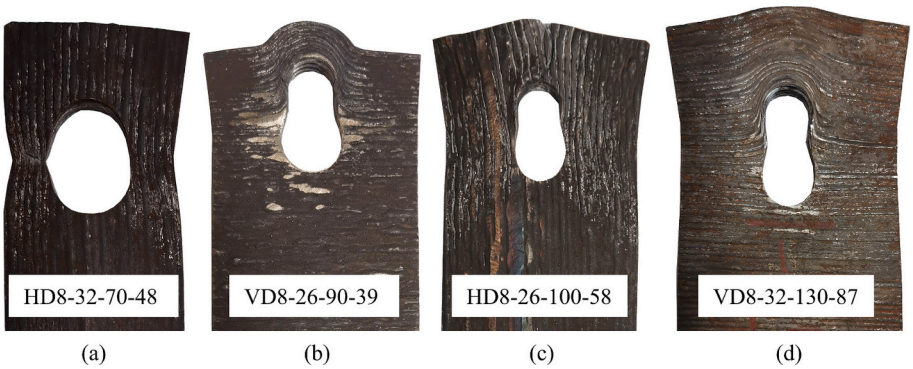

Fig. 9. Examples of failure modes: (a) net section tension, (b) shear-out, (c) end-splitting, (d) bearing.

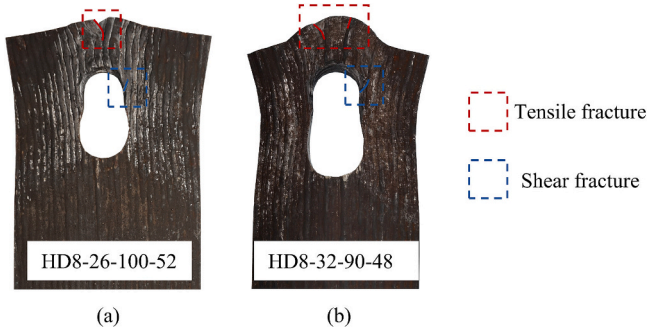

Fig. 10. Specimens exhibited a combination of shear-out and end-splitting failure.

experience shear-out failure. The print layers of VD specimens, aligned parallel to the direction of stress, conferred greater transverse resistance, leading to material accumulation in front of the bolt hole under bolt compression. In contrast, HD specimens, with their relatively lower transverse resistance, experienced fractures initiating from the plate end. This behaviour was also evident in specimen pairs No. 9 and 15.

For specimen pairs No. 5, 7, and 10, VD specimens tended to be more susceptible to net section tension failure, while HD specimens typically exhibited a greater likelihood of bearing failure. The underlying causes of this behaviour are discussed in detail in Section 4.1, which notes that the defects arising from the undulating surfaces of WAAM specimens induced the occurrence of net section tension failure.

Overall, the specimens with the same nominal dimensions but different print layer orientations exhibited clear anisotropy in terms of failure modes and ultimate capacities.

4.3. Analysis of thickness influence

To investigate the influence of the thickness of connected plates on the structural behaviours of WAAM steel bolted connections, a comparative analysis was conducted between the thin plates formed by single-layer feedstock wire in a previous study [19] and the thick plates formed by multi-layer feedstock wires in this study.

No interlayer slip between multiple feedstock wires was found in the cross-section of the WAAM steel specimen, which was consistent with the conventionally produced steel. However, the difference in ultimate capacity still needed to be analysed. Due to the lack of thin and thick WAAM steel connected plates with identical nominal geometric dimensions, the experimental results of specimens with the same e_1/d or e_2/d were compared. The normalized ultimate capacities F_u/Af_u represented the state in which the bolted connection structure exerted the cross-sectional strength of the connected plates. In Table 7, for bolted connections composed of thin and thick plates respectively, no general principle was found regarding the difference in normalized ultimate capacities between them. This may due to the small number of specimens with both the same e_1/d and e_2/d ratios.

When the e_1/d ratio of connected plates was the same, it was found that the average normalized ultimate capacities of bolted connections with thin plates were generally lower than those with thick plates, regardless of the end distance. The observed difference fluctuated between 0.01 and 0.12, as shown in Fig. 14(a). A similar trend was evident when comparing plates with the same e_2/d ratio, as shown in Fig. 14(b), with the exception of $e_2/d = 1.1$. These results suggest that bolted connections with thick plates more effectively utilize the cross-sectional strength of the material, providing more reliable performance.

4.4. Analysis of shear plane number influence

To examine the effect of the shear plane number on WAAM steel bolted connections, the structural behaviours of single-shear bolted connections and double-shear bolted connections were compared. Differences were observed in six pairs of single-shear and double-shear bolted connection specimens with the same nominal geometric dimensions, as shown in Table 8.

Bolted connection specimens with different shear plane numbers sometimes exhibited different failure modes. For example, specimen VD8–26–70-39 experienced shear-out failure, while specimen VS8–26–70-39 exhibited net section tension failure. The occurrence of this difference may be coincidental, as the theoretical ultimate capacities of these two failure modes (i.e., calculated based on their geometric dimensions of the connected plates) were similar, making both failure modes possible. Specimens HD8–26–70-39 and HS8–26–70-39 demonstrated a similar situation. In addition, specimens VS8–26–90-39 and VS8–32–90-48 showed different tilting-bearing failure modes compared to the corresponding double-shear bolted connection specimens. This discrepancy was due to the inability of single-shear bolted connections to prevent end plate curling, which ultimately led to tilt-bearing failure.

Despite these differences, the variations in the ultimate capacities were generally minor. The normalized ultimate capacities differences $\frac{F_{u,D}/tf_{u,D}}{F_{u,S}/tf_{u,S}}$ remained within 10 %. However, notable exceptions were observed in specimens VD8–26–90-39 and VS8–26–90-39, where the ratio was significantly lower at 0.84.

5. Comparisons of design predictions

5.1. General

This section evaluates the applicability of existing design equations outlined in Section 2. The evaluation involved comparing the observed failure modes and ultimate loads with the predictions from the design equations. The accuracy of the final failure modes predicted by three different standards was quantified by the failure mode prediction

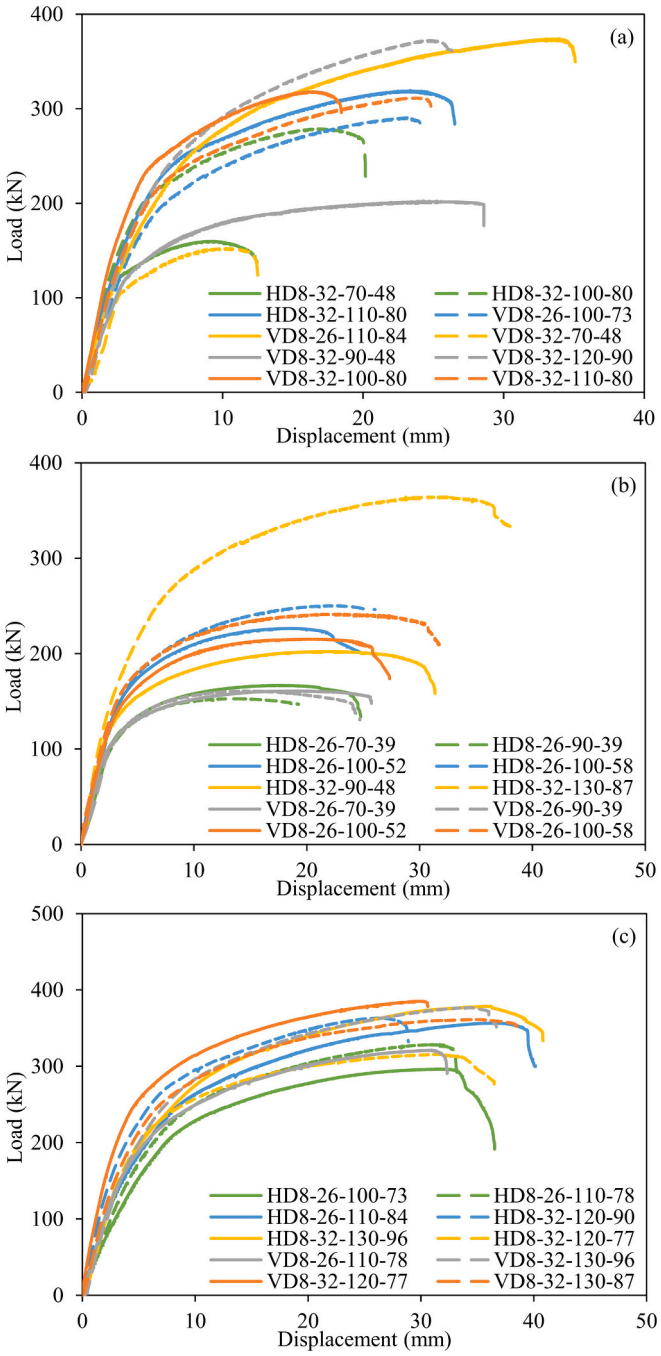

Fig. 11. The load-displacement curves of WAAM bolted connection specimens failed at different failure modes: (a) net section tension; (b) shear-out; (c) bearing.

accuracy (FMPA). In addition, the mean and coefficient of variation (COV) of the test-to-predicted capacity ratios for all design equations were also analysed and summarized in Fig. 15.

For the considered three standards, their FMPA varied from 0.40 to 0.73. AISC 360 [55] demonstrated the highest FMPA value of 0.73, while AS 4100 [52] recorded the lowest at 0.40. In terms of ultimate capacity prediction, AISC 360 [55] again excelled, with an average test-to-predicted capacity ratio of 1.03 and a COV of 0.09, underscoring its suitability for WAAM steel bolted connections. The performance predicted by the Eurocodes [53,54] was not far behind. Conversely, AS 4100 [52] not only struggled with failure mode prediction but also showed poor performance in predicting ultimate capacity.

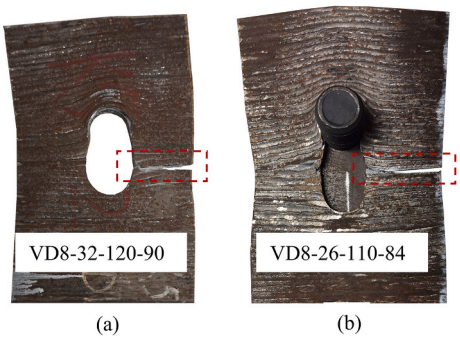

Fig. 12. Anomalous specimens: (a) VD8–32–120-90 and (b) VD8–26–110-84.

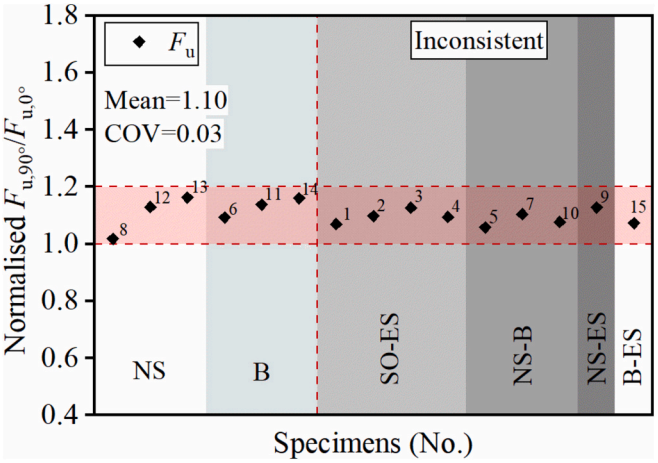

Fig. 13. Comparison of normalized ultimate capacities on different print layer orientations.

Table 7
Comparison of the experimental results of specimens with the same e_1/d and e_2/d.

e_1/d	e_2/d	F_u/Af_u	Specimen	Failure mode
1.5	1.7	0.42	HD8–26–90-39	SO/ES
		0.42	HD3–18–60-27	ES
1.5	1.1	0.53	VD8–32–70-48	NS
		0.56	VD3–18–40-27	NS
2.5	1.5	0.76	VD8–32–100-80	NS
		0.69	VD3–26–80-65	NS

Note: the edge distances e_2 was half the width b.

5.2. Ultimate capacities prediction for each failure mode

5.2.1. Net section tension failure

Given the potential influence of stress concentration effects, the full exertion of ultimate tensile strength at the critical net section may not be achievable. This consideration has led to the adoption of varying coefficients in different design provisions, with AS 4100 [52], AISC 360 [55], and Eurocode Eq. [53] employing coefficients of 0.85, 1, and 1 respectively.

The test-to-predicted capacity ratios of individual specimens failing by net section tension are summarized in Table 9. Occasionally, the specimens were incorrectly predicted to fail by shear-out or bearing failure, reducing the precision of failure mode predictions. Specifically, the accuracy of AS 4100 [52] did not surpass 50 %, which aligns with an average test-to-predicted capacity ratio of 1.28.

AISC 360 [55] and Eurocode [53] shared the same coefficient for net

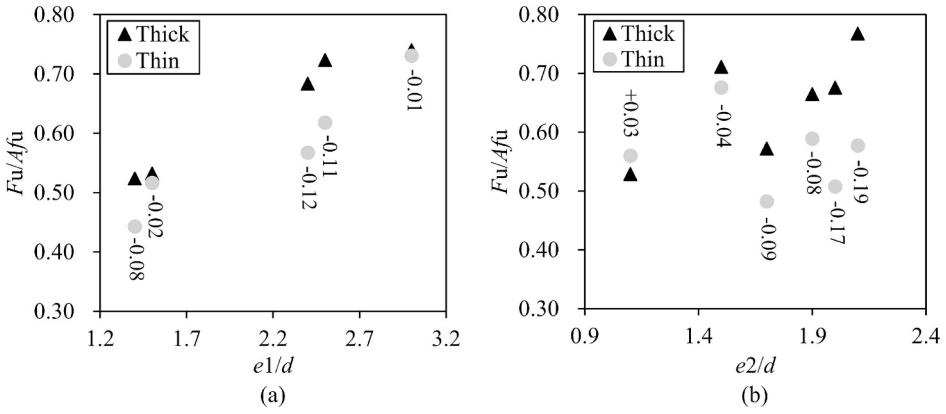

Fig. 14. Comparison of the normalized ultimate capacities of specimens with the same (a) e_1/d or (b) e_2/d.

Table 8
Comparison on experimental results of single- and double-shear bolted connection specimens.

Specimen (double-shear)	Failure mode	Specimen (single-shear)	Failure mode	$\frac{F_{u,D}/tf_{u,D}}{F_{u,S}/tf_{u,S}}$
HD8–26–70-39	SO/ES	HS8–26–70-39	NS	1.08
HD8–26–90-39	SO/ES	HS8–26–90-39	ES	0.92
HD8–32–90-48	SO/ES	HS8–32–90-48	ES	0.97
VD8–26–70-39	SO	VS8–26–70-39	NS	1.05
VD8–26–90-39	SO	VS8–26–90-39	TB	0.84
VD8–32–90-48	NS	VS8–32–90-48	TB	0.95

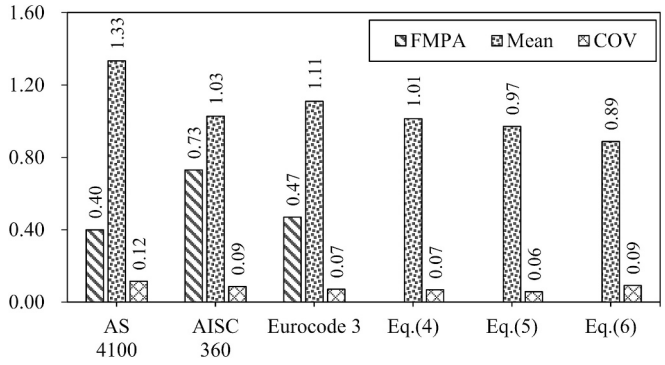

Fig. 15. Comparison between test results and predictions from existing design equations.

Table 9
Assessments of design codes for net section tension failure.

Specimen	FM	AS 4100		AISC 360		Eurocode 3	
		FM	F_u/F_{AS}	FM	F_u/F_{AISC}	FM	F_u/F_{EN3}
HD8–32–70-48	NS	(SO)	1.19	NS	0.98	NS	0.98
HD8–32–100-80	NS	NS	1.16	NS	0.98	NS	0.98
HD8–32–110-80	NS	(SO)	1.14	NS	0.91	(SO)	0.98
VD8–26–100-73	NS	(SO)	1.25	(B)	1.04	(SO)	1.11
VD8–26–110-84	NS	(SO)	1.29	(B)	1.27	(B)	1.27
VD8–32–70-48	NS	(SO)	1.20	NS	1.00	NS	1.00
VD8–32–90-48	NS	(SO)	1.67	(SO)	1.11	(SO)	1.19
VD8–32–120-90	NS	NS	1.24	NS	1.06	(SO)	1.10
VD8–32–100-80	NS	NS	1.31	NS	1.12	NS	1.12
VD8–32–110-80	NS	(SO)	1.33	NS	1.08	(SO)	1.13
FMPA		0.30		0.70		0.40	
Mean			1.28		1.06		1.09
COV			0.11		0.09		0.09

Note: failure mode in brackets means it was different from the test result.

section tension failure, yet the final predictions differed. For instance, HD8–32–110-80 was predicted to be a shear-out failure mode by Eurocode [53], because its theoretical ultimate capacity for net section tension failure was higher than that for shear-out failure. This discrepancy commonly occurred on specimens with a width exceeding 100 mm. In comparison, AISC 360 [55] provided more accurate predictions for both failure mode and ultimate capacity, achieving the highest FMPA of 0.70 and an average test-to-predicted capacity ratio of 1.06.

5.2.2. Shear-out/end-splitting failure

The absence of a distinct design equation for end-splitting failure may stem from current specifications' inability to make a clear distinction between shear-out and end-splitting failure. In the experiments, these two failure modes often occurred simultaneously in HD specimens. Given the similar mechanical behaviours exhibited by these two failure modes, many studies have used the design equations for shear-out failure to predict the ultimate capacities of end-splitting failure.

In Table 10, the ultimate capacities of all specimens subjected to end-splitting or shear-out failure were evaluated using the shear-out equation.

The superior predictive performance of AISC 360 [55] and Eq. (4) [44] was obvious, with their predictions being the most accurate ratio of 1.0. AISC 360 [55] overestimated the ultimate capacity by 1.0 %, while Eq. (4) [44] underestimated the ultimate capacity by 1.0 %. In practical applications, a conservative prediction for design code is generally preferred, therefore, Eq. (4) [44] is recommended.

5.2.3. Bearing failure

For AS 4100 [52], due to the utilization of a smaller shear coefficient in the design equation of shear-out failure, the calculated ultimate capacities were relatively small and the predicted failure modes were shear-out, as shown in Table 11. It caused an extremely low FMPA of AS 4100 [52] with a poor average test-to-predicted capacity ratio of 1.26. The Eurocode Eq. [54] also led to a similar situation. Differently, AISC 360 [55] provided the most accurate predictions with an FMPA of 0.7 and an average test-to-predicted capacity ratio of 1.04.

For the proposed Eq. (6) [38] in recent literature, the average ultimate capacity prediction resulted in an overestimation of 16 %, indicating that the adopted bearing coefficient of 3.5 was still too high for WAAM steel bolted connection.

5.3. Comparison with other bolted connections

Previous research [19] found that existing design provisions for conventionally manufactured steel had certain applicability for WAAM steel bolted connections composed of thin plates. Fig. 16 compares the prediction performance of WAAM bolted connections composed of thin and thick plates.

Table 10
Assessments of design codes for shear-out/end-splitting failure.

Specimen	FM	AS 4100		AISC 360		Eurocode 3		Eq. (4)	Eq. (5)
		FM	F_u/F_{AS}	FM	F_u/F_{AISC}	FM	F_u/F_{EN3}	$F_u/F_{Eq.(4)}$	$F_u/F_{Eq.(5)}$
HD8–26–70-39	SO/ES	SO	1.52	SO	1.02	SO	1.10	1.02	0.96
HD8–26–90-39	SO/ES	SO	1.43	SO	0.96	SO	1.04	0.96	0.90
HD8–26–100-52	SO/ES	SO	1.34	SO	0.89	SO	1.09	0.96	0.92
HD8–26–100-58	ES	(SO)	1.34	(SO)	0.89	(SO)	1.12	0.97	0.95
HD8–32–90-48	SO/ES	SO	1.52	SO	1.02	SO	1.08	1.01	0.95
HD8–32–130-87	SO/ES	SO	1.19	(B)	0.93	SO	1.05	0.89	0.89
VD8–26–70-39	SO	SO	1.64	SO	1.10	SO	1.18	1.10	1.03
VD8–26–90-39	SO	SO	1.62	SO	1.08	SO	1.17	1.08	1.01
VD8–26–100-52	SO	SO	1.51	SO	1.01	SO	1.23	1.08	1.04
VD8–26–100-58	SO	SO	1.45	SO	0.97	SO	1.21	1.06	1.03
FMPA		0.90		0.80		0.90			
Mean			1.46		0.99		1.13	1.01	0.97
COV			0.09		0.07		0.06	0.06	0.06

Table 11
Assessments of design codes for bearing failure.

Specimen	FM	AS 4100		AISC 360		Eurocode 3		Eq. (6)
		FM	FM	F_u/F_{AS}	FM	F_u/F_{AISC}	FM	$F_u/F_{Eq.(6)}$
HD8–26–100-73	B	(SO)	1.19	B	0.98	(SO)	1.06	0.84
HD8–26–110-78	B	(SO)	1.21	B	1.07	(SO)	1.09	0.92
HD8–26–110-84	B	(SO)	1.19	B	1.15	B	1.15	0.98
HD8–32–120-90	B	(SO)	1.18	(NS)	0.97	(SO)	1.04	0.82
HD8–32–130-96	B	(SO)	1.14	B	1.01	(SO)	1.02	0.87
HD8–32–120-77	B	(SO)	1.27	(NS)	0.87	(SO)	1.08	0.74
VD8–26–110-78	B	(SO)	1.32	B	1.17	(SO)	1.19	1.01
VD8–32–130-96	B	(SO)	1.33	B	1.15	(SO)	1.17	0.99
VD8–32–120-77	B	(SO)	1.48	(NS)	1.02	(SO)	1.26	0.85
VD8–32–130-87	B	(SO)	1.28	B	1.00	(SO)	1.11	0.86
FMPA		0.00		0.70		0.10		
Mean			1.26		1.04		1.12	0.89
COV			0.08		0.09		0.06	0.09

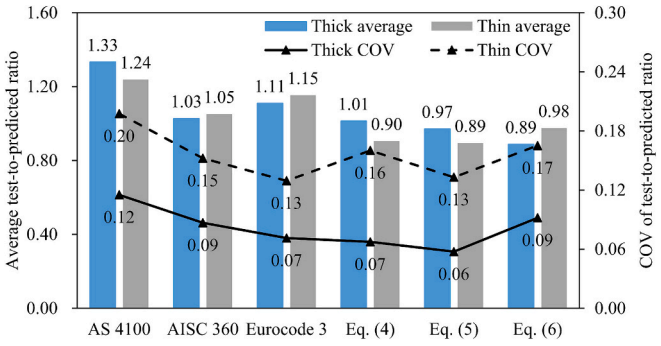

Fig. 16. Prediction performance comparison of bolted connections composed of thin and thick plates.

In terms of the average test-to-predicted ratio of each design provision, there was no clear pattern indicating differences in the applicability of WAAM steel bolted connections composed of thick and thin plates. AISC 360 showed the smallest variation, showing the least influence from plate thickness. In addition, the COVs of thick plates were generally smaller than those of thin plates.

Overall, it could be assumed that the thickness of connected plates of WAAM bolted connections had a slight influence on the prediction results, and the prediction on thick plates was more stable.

A prediction performance comparison was also conducted between the presented experimental study and the results by Guo et al. [49] to assess whether significant differences exist in similar components printed in different regions by various researchers. The results of this comparison are shown in Fig. 17. Overall, the average and COV of the test-to-predicted ratios in both studies are quite similar, with results presented in the current paper demonstrating slightly better predictive performance. However, in predicting the ultimate capacities of bolted connection specimens with net section tension failure, Guo et al. [49] shows better stability, as reflected in generally lower COV values. For specimens with shear-out and end-splitting failures, predictions across design codes, except for AS 4100 [52] and AISC 360 [55], are notably consistent. In summary, the differences among researchers' results are relatively small, supporting the future development of design stipulations for WAAM bolted connections.

6. Conclusions

This study tested 30 WAAM double-shear bolted connection specimens, each with distinct print layer orientations and geometric dimensions. The research thoroughly analysed and discussed the influence of print layer orientations on the performance of WAAM steel bolted connections. Based on the experimental results, an evaluation of existing design provisions for conventionally manufactured steel bolted connections was conducted based on the experimental results. The research led to the following key conclusions:

1) The experiment found that the material properties of WAAM steel generally decreased with increasing printing orientation θ. However, in the tests of WAAM steel bolted connections, VD specimens ($\theta = 90°$) generally exhibited higher ultimate capacities compared to HD specimens ($\theta = 0°$).
2) Four distinct failure modes were observed in the WAAM double-shear bolted connection specimens: net section tension, shear-out, end-splitting, and bearing failure. The print layer orientation significantly influenced both the failure modes and the ultimate

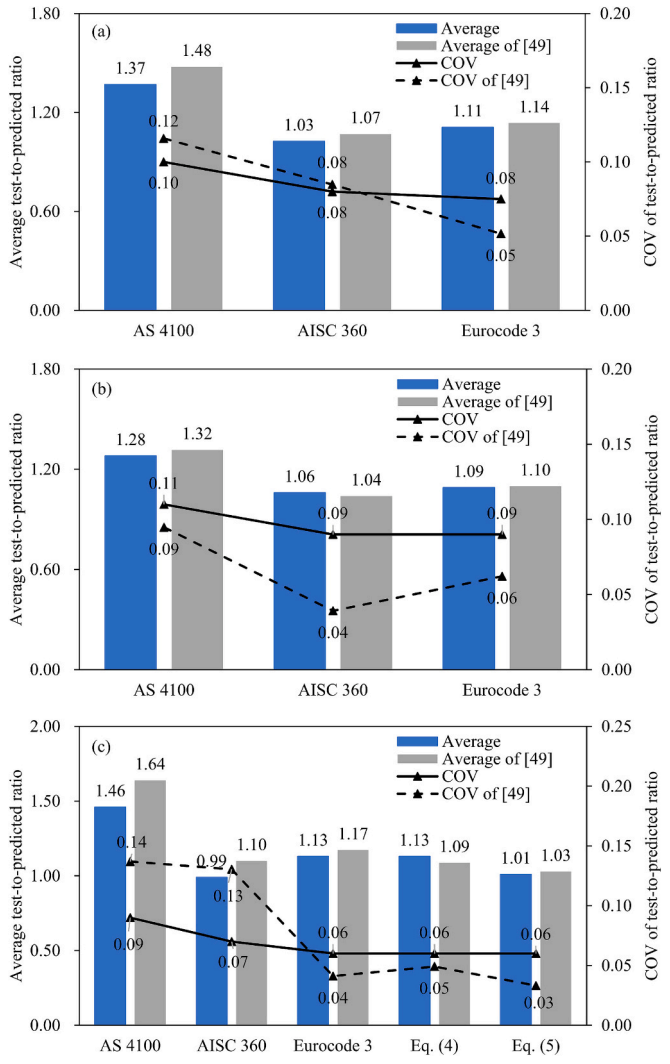

Fig. 17. Comparison of prediction performance for bolted connections in this research and the results presented by Guo et al. [49] across different failure modes: (a) overall, (b) net section tension, (c) shear-out/end-splitting.

capacities. Specifically, HD specimens were more prone to end-splitting, while VD specimens were more likely to experience net section tension failure.

3) Existing design provisions for conventionally manufactured steel bolted connections were used to evaluate the ultimate capacities of the tested WAAM specimens. AISC 360 [55] excelled with the highest failure mode prediction accuracy of 0.73, an average test-to-predicted capacity ratio of 1.03 and a coefficient of variation (COV) of 0.09. AISC 360 [55] also provided the most accurate ultimate load predictions for all four failure modes, indicating its suitability for WAAM steel bolted connections.
4) Bolted connections composed of thick plates better utilized the cross-sectional strength of the material and provided more reliable performance. Compared with connections composed of WAAM thin plates, those of thick plates exhibited greater stability during tests and showed better compatibility with existing design provisions.
5) While the existing design provisions provide valuable guidance, they fall short of accurately identifying the end-splitting failure mode, highlighting the need for a design provision tailored to WAAM steel. Moreover, further scholarly investigation is essential to advance the practical application of 3D printing technology in engineering projects.

CRediT authorship contribution statement

Yunyi Liu: Writing – original draft, Validation, Methodology, Investigation, Formal analysis. **Jun Ye:** Writing – review & editing, Supervision, Investigation, Funding acquisition, Conceptualization. **Jiangfei He:** Writing – review & editing, Supervision. **Hongjia Lu:** Writing – review & editing, Validation, Supervision, Investigation. **Guan Quan:** Writing – review & editing, Supervision, Resources, Project administration, Funding acquisition, Formal analysis. **Zhen Wang:** Writing – review & editing, Supervision. **Yang Zhao:** Writing – review & editing, Supervision, Investigation, Funding acquisition, Conceptualization.

Declaration of competing interest

The authors declare that they have no known competing financial interests or personal relationships that could have appeared to influence the work reported in this paper.

Data availability

The data presented in this work will be made available upon reasonable request.

Acknowledgement

The authors would like to acknowledge the financial support to this project by the National Natural Science Foundation of China (No. 52078452, 52208215), the Basic Public Research Project of Zhejiang Province (No. LGG22E080005, LQ22E080008).

References

[1] L. Gardner, Metal additive manufacturing in structural engineering – review, advances, opportunities and outlook, Structures 47 (2023) 2178–2193.
[2] J. Ye, P. Kyvelou, F. Gilardi, H. Lu, M. Gilbert, L. Gardner, An end-to-end framework for the additive manufacture of optimized tubular structures, IEEE Access. 9 (2021) 165476–165489.
[3] A. Kanyilmaz, A.G. Demir, M. Chierici, F. Berto, L. Gardner, S.Y. Kandukuri, P. Kassabian, T. Kinoshita, A. Laurenti, I. Paoletti, A. du Plessis, N. Razavi, Role of metal 3D printing to increase quality and resource-efficiency in the construction sector, Addit. Manuf. 50 (2022) 102541.
[4] V. Laghi, G. Gasparini, Explorations of efficient design solutions for wire-and-arc additive manufacturing in construction, Structures 56 (2023) 104883.
[5] T. Feucht, B. Waldschmitt, J. Lange, M. Erven, Additive manufacturing of a bridge in situ, Steel Construct. 15 (2022) 100–110.
[6] L. Gardner, P. Kyvelou, G. Herbert, C. Buchanan, Testing and initial verification of the world's first metal 3D printed bridge, J. Constr. Steel Res. 172 (2020) 106233.
[7] N. Hadjipantelis, I.H. Shah, L. Walter, R.J. Myers, L. Gardner, Metal additively versus conventionally manufactured structures – an environmental life cycle assessment, ce/papers. 6 (2023) 672–677.
[8] S.I. Evans, J. Wang, J. Qin, Y. He, P. Shepherd, J. Ding, A review of WAAM for steel construction – manufacturing, material and geometric properties, design, and future directions, Structures 44 (2022) 1506–1522.
[9] P. Kyvelou, A. Spinasa, L. Gardner, Testing and analysis of optimized wire arc additively manufactured steel trusses, J. Struct. Eng. 150 (2024).
[10] J. Lange, T. Feucht, M. Erven, 3D-printing with steel - additive manufacturing connections and structures, ce/papers. 4 (2021) 2–7.
[11] T. Feucht, B. Waldschmitt, J. Lange, M. Erven, 3D-printing with steel: additive manufacturing of a bridge in situ, ce/papers. 4 (2021) 1695–1701.
[12] C. Huang, P. Kyvelou, R. Zhang, T. Ben Britton, L. Gardner, Mechanical testing and microstructural analysis of wire arc additively manufactured steels, Mater. Des. 216 (2022) 110544.
[13] N. Hadjipantelis, B. Weber, C. Buchanan, L. Gardner, Description of anisotropic material response of wire and arc additively manufactured thin-walled stainless steel elements, Thin-Walled Struct. 171 (2022) 108634.
[14] P. Kyvelou, H. Slack, C. Buchanan, M.A. Wadee, L. Gardner, Material testing and analysis of WAAM stainless steel 4 (2021) 1702–1709.
[15] V. Laghi, M. Palermo, G. Gasparini, V.A. Girelli, T. Trombetti, On the influence of the geometrical irregularities in the mechanical response of wire-and-arc additively manufactured planar elements, J. Constr. Steel Res. 178 (2021) 106490.
[16] V. Laghi, L. Arrè, L. Tonelli, G. Di Egidio, L. Ceschini, I. Monzón, A. Laguía, J. A. Dieste, M. Palermo, Mechanical and microstructural features of wire-and-arc additively manufactured carbon steel thick plates, Int. J. Adv. Manuf. Technol. 127 (2023) 1391–1405.

[17] C. Huang, L. Li, N. Pichler, E. Ghafoori, L. Susmel, L. Gardner, Fatigue testing and analysis of steel plates manufactured by wire-arc directed energy deposition, Addit. Manuf. 73 (2023) 103696.
[18] J. Ye, Y. Liu, Y. Yang, Z. Wang, O. Zhao, Y. Zhao, Testing, analysis and design of wire and arc additively manufactured steel bolted connections, Eng. Struct. 296 (2023).
[19] Y. Liu, J. Ye, Y. Yang, G. Quan, Z. Wang, W. Zhao, Y. Zhao, Experimental study on wire and arc additively manufactured steel double-shear bolted connections, J. Build. Eng. 76 (2023) 107330.
[20] M.-T. Chen, T. Zhang, Z. Gong, W. Zuo, Z. Wang, L. Zong, O. Zhao, L. Hu, Mechanical properties and microstructure characteristics of wire arc additively manufactured high-strength steels, Eng. Struct. 300 (2024).
[21] T.J. Dodwell, L.R. Fleming, C. Buchanan, P. Kyvelou, G. Detommaso, P.D. Gosling, R. Scheichl, W.S. Kendall, L. Gardner, M.A. Girolami, C.J. Oates, A data-centric approach to generative modelling for 3D-printed steel, Proc. Math. Phys. Eng. Sci. 477 (2021) 20210444.
[22] J. Müller, J. Hensel, K. Dilger, Correction to: mechanical properties of wire and arc additively manufactured high-strength steel structures, Weld. World 66 (2022) 1067–1068.
[23] J. Ge, J. Lin, Y. Long, Q. Liu, L. Zhang, W. Chen, Y. Lei, Microstructural evolution and mechanical characterization of wire arc additively manufactured 2Cr13 thin-wall part, J. Mater. Res. Technol. 13 (2021) 1767–1778.
[24] V. Laghi, L. Tonelli, M. Palermo, M. Bruggi, R. Sola, L. Ceschini, T. Trombetti, Experimentally-validated orthotropic elastic model for wire-and-arc additively manufactured stainless steel, Addit. Manuf. 42 (2021) 101999.
[25] L. Tonelli, R. Sola, V. Laghi, M. Palermo, T. Trombetti, L. Ceschini, Influence of interlayer forced air cooling on microstructure and mechanical properties of wire arc additively manufactured 304L austenitic stainless steel, Steel Res. Int. 92 (2021) 2100175.
[26] C. Huang, P. Kyvelou, L. Gardner, Stress-strain curves for wire arc additively manufactured steels, Eng. Struct. 279 (2023) 115628.
[27] V. Laghi, M. Palermo, G. Gasparini, V.A. Girelli, T. Trombetti, Experimental results for structural design of wire-and-arc additive manufactured stainless steel members, J. Constr. Steel Res. 167 (2020) 105858.
[28] P. Kyvelou, C. Huang, L. Gardner, C. Buchanan, Structural testing and design of wire arc additively manufactured square hollow sections, J. Struct. Eng. 147 (2021) 04021218.
[29] C. Huang, X. Meng, C. Buchanan, L. Gardner, Flexural buckling of wire arc additively manufactured tubular columns, J. Struct. Eng. 148 (2022) 04022139.
[30] C. Huang, X. Meng, L. Gardner, Cross-sectional behaviour of wire arc additively manufactured tubular beams, Eng. Struct. 272 (2022) 114922.
[31] X. Guo, P. Kyvelou, J. Ye, L. Gardner, Experimental investigation of wire arc additively manufactured steel T-stub connections, J. Constr. Steel Res. 211 (2023) 108106.
[32] M. Erven, J. Lange, T. Feucht, 3D-printing with steel of a bolted connection, ce/papers 4 (2021) 825–832.
[33] S. Evans, N. Hadjipantelis, J. Wang, Effects of deposition rate on local stability of wire arc additively manufactured outstand elements, ce/papers. 6 (2023) 678–683.
[34] S. Evans, J. Wang, J. Pan, F. Xu, Experimental study of wire arc additively manufactured steel sections stiffened by sinusoidal waves, Structures 65 (2024).
[35] S.I. Evans, F. Xu, J. Wang, Experiments on the material and stability performance of slender WAAM plated structures, Thin-Walled Struct. 202 (2024).
[36] C. Ding, S. Torabian, B.W. Schafer, Strength of bolted lap joints in steel sheets with small end distance, J. Struct. Eng. 146 (2020) 04020270.
[37] A.G. Kamtekar, On the bearing strength of bolts in clearance holes, J. Constr. Steel Res. 79 (2012) 48–55.
[38] L.H. Teh, M.E. Uz, Combined bearing and shear-out capacity of structural steel bolted connections, J. Struct. Eng. 142 (2016) 04016098.
[39] M.D. Elliott, L.H. Teh, A. Ahmed, Behaviour and strength of bolted connections failing in shear, J. Constr. Steel Res. 153 (2019) 320–329.
[40] P. Može, Bearing strength at bolt holes in connections with large end distance and bolt pitch, J. Constr. Steel Res. 147 (2018) 132–144.
[41] L.H. Teh, B.P. Gilbert, Net section tension capacity of bolted connections in cold-reduced steel sheets, J. Struct. Eng. 138 (2012) 337–344.
[42] E.L. Salih, L. Gardner, D.A. Nethercot, Numerical investigation of net section failure in stainless steel bolted connections, J. Constr. Steel Res. 66 (2010) 1455–1466.
[43] L.H. Teh, D.D.A. Clements, Block shear capacity of bolted connections in cold-reduced steel sheets, J. Struct. Eng. 138 (2012) 459–467.
[44] L.H. Teh, M.E. Uz, Ultimate shear-out capacities of structural-steel bolted connections, J. Struct. Eng. 141 (2015) 04014152.
[45] H. Xing, L.H. Teh, Z. Jiang, A. Ahmed, Shear-out capacity of bolted connections in cold-reduced steel sheets, J. Struct. Eng. 146 (2020) 04020018.
[46] D.D.A. Clements, L.H. Teh, Active shear planes of bolted connections failing in block shear, J. Struct. Eng. 139 (2013) 320–327.
[47] H. Teh Lip, Mehmet E. Uz, Ultimate tilt-bearing capacity of bolted connections in cold-reduced steel sheets, J. Struct. Eng. 143 (2017) 04016206.
[48] X. Guo, P. Kyvelou, J. Ye, L.H. Teh, L. Gardner, Experimental investigation of wire arc additively manufactured steel single-lap shear bolted connections, Thin-Walled Struct. 181 (2022) 110029.
[49] X. Guo, P. Kyvelou, J. Ye, L.H. Teh, L. Gardner, Experimental study of DED-arc additively manufactured steel double-lap shear bolted connections, Eng. Struct. 281 (2023) 115736.
[50] W. Zuo, M.-T. Chen, S.-W. Liu, X. Yun, O. Zhao, Y. Huang, B. Cheng, Experimental investigation on double-lap shear behavior of 3D printed austenitic stainless steel bolted connections, Eng. Struct. 317 (2024) 118501.
[51] W. Zuo, M.-T. Chen, O. Zhao, A. Su, S.-W. Liu, F. Xu, Y. Huang, B. Cheng, Behavior of wire arc additively manufactured 316L austenitic stainless steel single shear bolted connections, Thin-Walled Struct. 202 (2024) 112075.
[52] AS 4100, Steel Structures, Standards Association of Australia, Australia, 2020.
[53] Eurocode 3 - Design of Steel Structures – Part 1–1: General Rules and Rules for Builidng, European Committee for Standardisation, Brussels, 2020.
[54] Eurocode 3 - Design of Steel Structures – Part 1-8: Joints, European Committee for Standardisation, Brussels, 2024.
[55] AISC 360, Specification for Structural Steel Buildings, American Institute of Steel Construction, Chicago, 2022.
[56] AS/NZS 4600, Cold-Formed Steel Structures, Australian/New Zealand Standard, Sydney, 2018.